Journal of Power Sources 188 (2009) 114–117

Contents lists available at ScienceDirect

Journal of Power Sources

journal homepage: www.elsevier.com/locate/jpowsour

Short communication

Synthesis of nano-crystalline $Sr_2MgMoO_{6-\delta}$ anode material by a sol–gel thermolysis method

Lingcai Kong[a], Bangwu Liu[a], Jing Zhao[a], Yousong Gu[a], Yue Zhang[a,b,c,*]

[a] Department of Materials Physics, University of Science and Technology Beijing, Beijing 100083, People's Republic of China
[b] Key Laboratory of New Energy Materials and Technologies, University of Science and Technology Beijing, Beijing 100083, People's Republic of China
[c] State Key Laboratory For Advanced Metals And Materials, University of Science and Technology Beijing, Beijing 100083, People's Republic of China

ARTICLE INFO

Article history:
Received 8 October 2008
Received in revised form
24 November 2008
Accepted 24 November 2008
Available online 11 December 2008

Keywords:
$Sr_2MgMoO_{6-\delta}$ (SMMO)
Sol–gel thermolysis method
Crystal structure
Conductivity

ABSTRACT

Nano-crystalline $Sr_2MgMoO_{6-\delta}$ (SMMO) powders were synthesized successfully by a novel sol–gel thermolysis method using a unique combination of polyvinyl alcohol (PVA) and urea. The decomposition behavior of gel precursor was studied by thermogravimetric-differential thermal analysis (TG/DTA) and the results showed that the double-perovskite phase of SMMO began to form at 1000 °C. The microstructure of the samples had been investigated by X-ray diffraction (XRD), transmission electron microscope (TEM), selected area electron diffraction (SAED), Raman spectroscopy and X-ray photoelectron spectroscopy (XPS). XRD patterns confirmed that well-crystalline double-perovskite SMMO powders were obtained by calcining at 1450 °C for 12 h. TEM morphological analysis showed that SMMO powders had a mean particle size around 50–100 nm. The SAED pattern and Raman spectroscopy showed that the SMMO powders were nano-polycrystalline well-developed $A(B'_{0.5}B''_{0.5})O_3$ type perovskite material. The XPS results demonstrated that the Mo ions in SMMO had been reduced after exposure to H_2. The electric property was studied by four-probe method. The results showed that conductivity was 8.64 S cm^{-1} in 5.0% H_2/Ar at 800 °C and the activation energies at low temperatures (400–640 °C) and high temperatures (640–800 °C) are about 21.43 and 6.59 kJ mol^{-1}, respectively.

© 2008 Elsevier B.V. All rights reserved.

1. Introduction

Solid oxide fuel cells (SOFCs) are promising for stationary and distributed energy conversion devices that exhibit various advantages, such as high efficiency, system compactness and low environmental pollution [1]. They offer an opportunity for direct utilization of hydrocarbons as fuels, such as natural gas, which makes them more competitive in comparison with other fuel cell systems. Conventional SOFC generally operates at 1000 °C, which seriously limits its application. Therefore, a common trend recently is to develop intermediate-temperature solid oxide fuel cells (IT-SOFC), which can be operated at a moderate temperature, especially below 800 °C [2,3]. In order to improve the performance of IT-SOFC, a group of new materials have been investigated, including anode materials.

The most commonly used anode materials for SOFCs are Ni/YSZ cermets, which exhibit excellent catalytic activity towards hydrogen fuel oxidation as well as good current collection. However, it also has some disadvantages, such as poor redox stability, carbon deposition and sulphur poisoning when hydrocarbon fuels are used, and the tendency of agglomeration of Ni particles after prolonged operation [4]. Therefore, various new anode materials with different crystal structures have been investigated to solve those problems while keeping good electrochemical performance, such as rutile, fluorite, perovskite, pyrochlore and tungsten bronze. Amongst them, the perovskite-type oxides, which are chemically stable under fuel conditions, have received much attention and yielded promising results [5,6]. $Sr_2MgMoO_{6-\delta}$ (SMMO), as one of the perovskite anode systems, has recently shown excellent performance, high redox and chemical stability, high resistance to poisoning by sulfur impurities, good electronic conductivity and electrocatalytic activity in reducing atmosphere [7,8]. However, Lopez et al. have reported that SMMO phase presents limited redox stability at temperatures above 900 °C, and the synthesis of SMMO by standard ceramic route requires long sintering time of 44 h [9]. Consequently, the grain size increases at high sintering temperature, which will degrade the performance of the anode material.

In this study, the SMMO powders for anode materials were synthesized by a novel temperature sol–gel thermolysis method. The crystal structures and electrochemical performance were studied in detail.

* Corresponding author at: Department of Materials Physics, University of Science and Technology Beijing, Beijing 100083, People's Republic of China.
Tel.: +86 10 62334725; fax: +86 10 62333113.
E-mail address: yuezhang@ustb.edu.cn (Y. Zhang).

0378-7753/$ – see front matter © 2008 Elsevier B.V. All rights reserved.
doi:10.1016/j.jpowsour.2008.11.134

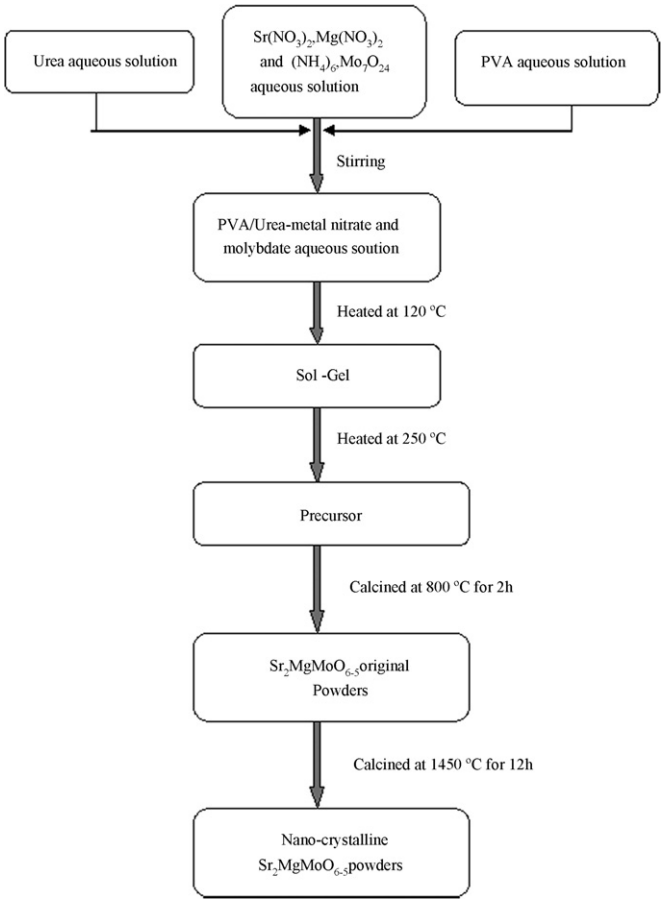

Fig. 1. Flowchart for the synthesis of nano-crystalline SMMO powders by sol–gel thermolysis method.

2. Experimental

2.1. Synthesis of SMMO powders

Nano-crystalline SMMO powders were synthetized by a novel sol–gel thermolysis method using urea as the fuel of combustion process and PVA as the dispersing agent as well as secondary fuel. $Sr(NO_3)_2$, $Mg(NO_3)_2{\cdot}6H_2O$, $(NH_4)_6Mo_7O_{24}{\cdot}4H_2O$ were used as the starting materials. All the starting materials were analytical reagent grade (Beijing Yili Chemicals Co. Ltd., China). The procedure for synthesis of nano-crystalline SMMO powders is outlined in Fig. 1. Stoichiometric amount of $Sr(NO_3)_2$, $Mg(NO_3)_2{\cdot}6H_2O$ and $(NH_4)_6Mo_7O_{24}{\cdot}4H_2O$ were dissolved in distilled water to obtain transparent solutions. Then, aqueous solution of PVA and urea were added to the desired proportions with constant stirring until a homogeneous solution was achieved. The mixed solution was heated to 120 °C in a baker to obtain a viscous solution (sol). The viscous solution was further heated to 250 °C to obtain the precursor sample (gel) until combustion. The as-synthesized precursor was then calcined at 800 °C for 2 h in air to decompose the redundant organic compounds. Finally, the as-synthetized powders were pressed into a rectangular bar at about 200 MPa followed by sintering at 1450 °C in air for 12 h to obtain a well-crystallized dense bar.

2.2. Characterizations

The reaction temperatures were measured by a TG/DTA thermal analyzer (Model:TG/DTA PYRIS DIAMOND) in air-flow with a temperature rate of 10 °C/min. XRD using Cu Kα radiation was carried out to identify phase formation on a Rigaku Dmax-RB X-ray diffractometer at a scanning speed of 0.02° per step. The morphology of the calcined powders was observed in a transmission electron microscope (JEM-1OOCX). XPS spectra were recorded on a MK II photoelectron spectrometer with a monochromated and microfocused Mg Kα ($h\nu$ = 1253.6 eV) X-ray source. Raman spectra were obtained using a JYT6400 Raman spectromicroscope. The electrical conductivity of the sintered sample was measured by DC four-probe method in H_2 from 400 to 800 °C with a step of 20 °C. A constant current in the range of 1 μA to 1 A was applied, and the voltage was recorded using a KEITHLEY 2410 source meter.

3. Results and discussion

3.1. TG/DTA analysis

Fig. 2 shows the TG/DTA curves of the SMMO precursor synthesized by a sol–gel thermolysis method. The weight loss over the temperature range of 240–350 °C corresponds to the removal of superficial and structural water in the gel precursor, which is correlated to the small endothermic peak at 250 °C in the DTA curve. The weight loss between approximately 700 and 950 °C is associated with the complex decomposition reactions of organics and metal nitrates, accompanied by the exothermic peaks at 785 and 920 °C in the DTA curve. The weight gain from 980 to 1100 °C is due to the reactions between various metal oxides and oxygen in the air, which denotes the onset of structural transition, corresponding to the small endothermic peak at 1000 °C in the DTA curve. This would be further confirmed by XRD measurements.

3.2. Structure characterizations

The X-ray diffraction (XRD) patterns of SMMO powders calcined at different temperatures for 12 h are shown in Fig. 3. The results show that double-perovskite type SMMO phase ($Fm\bar{3}m$) has formed at 1000 °C, which conforms to the TG-DTA results well. However, the diffraction peaks are broad, and there exists a small amount of impurity phases below 1450 °C. The amount of impurity phases decreases and the diffraction peaks become sharper and higher when the calcination temperatures increase. The powders are crystallized into pure double-perovskite with no impurity formatted after calcined at 1450 °C for 12 h. This duration is relatively shorter than that of conventional solid-state reaction method with sintering time of 44 h [7].

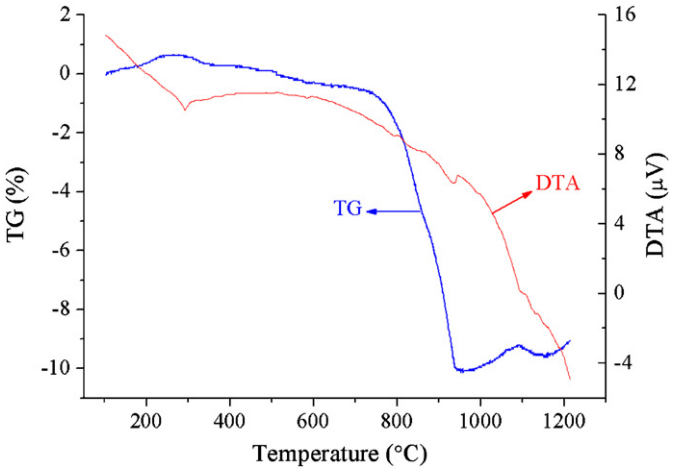

Fig. 2. TG-DTA curves of the SMMO precursor synthesized by sol–gel thermolysis method.

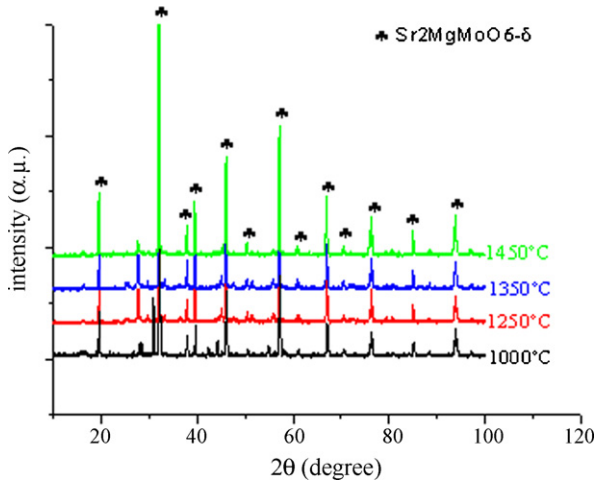

Fig. 3. XRD patterns for SMMO powders calcined at different temperatures for 12 h.

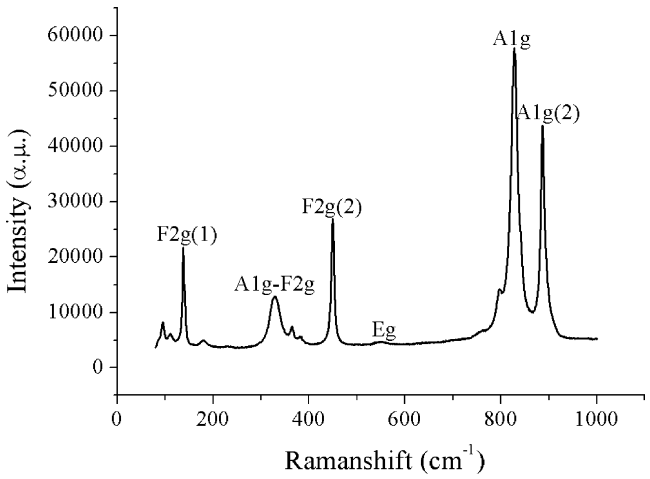

Fig. 5. Raman spectroscopy of as-prepared SMMO rectangular bar.

TEM image and SAED pattern of SMMO powders after pre-calcined at 1450 °C for 12 h are shown in Fig. 4. The TEM observation reveals that the obtained SMMO powders have a mean grain size around 50–100 nm. The SAED pattern indicates that the as-calcined powders are well-developed polycrystalline material.

It is well reported that $A(B'_{0.5}B''_{0.5})O_3$ type complex perovskite structure has four active Raman modes at room temperature: A_{1g}, E_g, $F_{2g(1)}$, $F_{2g(2)}$ [10]. Fig. 5 shows the Raman spectroscopy of SMMO rectangular bar sintered at 1450 °C for 12 h. The bands at 137 and 449 cm^{-1} are assigned to the $F_{2g(1)}$ and $F_{2g(2)}$ modes. The bands at 94 and 110 cm^{-1} are most likely to be the triply degenerated $F_{2g(1)}$ mode. The line spilt in the $F_{2g(2)}$ mode is reported for many complex perovskite materials, such as $Sr(Nd_{0.5}Nb_{0.5})$ and $Sr(La_{0.5}Ta_{0.5})O_3$ by Ratheesh et al. [10]. The band in region 310–360 cm^{-1} shows up because of different ionic radii at the B-site and deviation from a perfect cubic structure. The band at 380 cm^{-1} is A_{1g} (at 828 cm^{-1}) – F_{2g} (at 449 cm^{-1}). The weak band at 520 cm^{-1} is assigned to the E_g mode. An additional feature appears in the Raman spectra of SMMO when the A_{1g} mode spilt into two intensive modes at 828 and 886 cm^{-1}. The mode at 798 cm^{-1} is not so intensive because of the lower tolerance factor observed in the splitting of A_{1g} mode. The above results clearly indicate that SMMO perovskite material shows four active Raman modes: A_{1g}, E_g, $F_{2g(1)}$, $F_{2g(2)}$, which shows that the structure of as prepared SMMO is in good agreement with $A(B'_{0.5}B''_{0.5})O_3$ type complex perovskite structure.

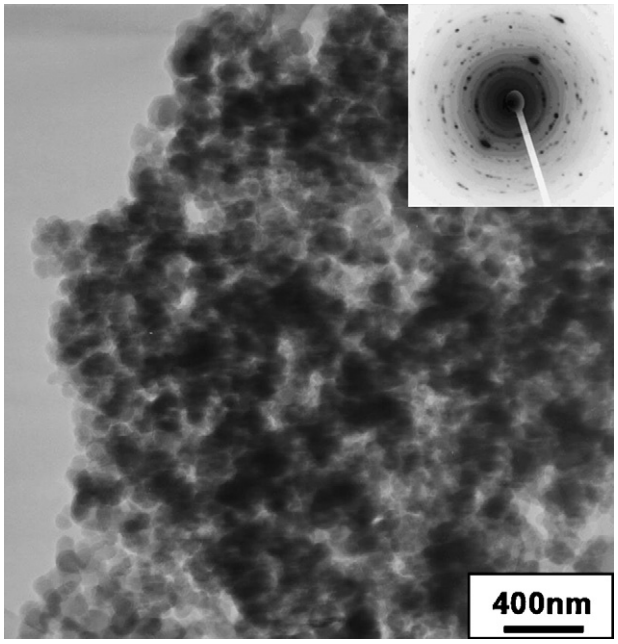

Fig. 4. TEM image and SAED pattern of as-calcined SMMO powders.

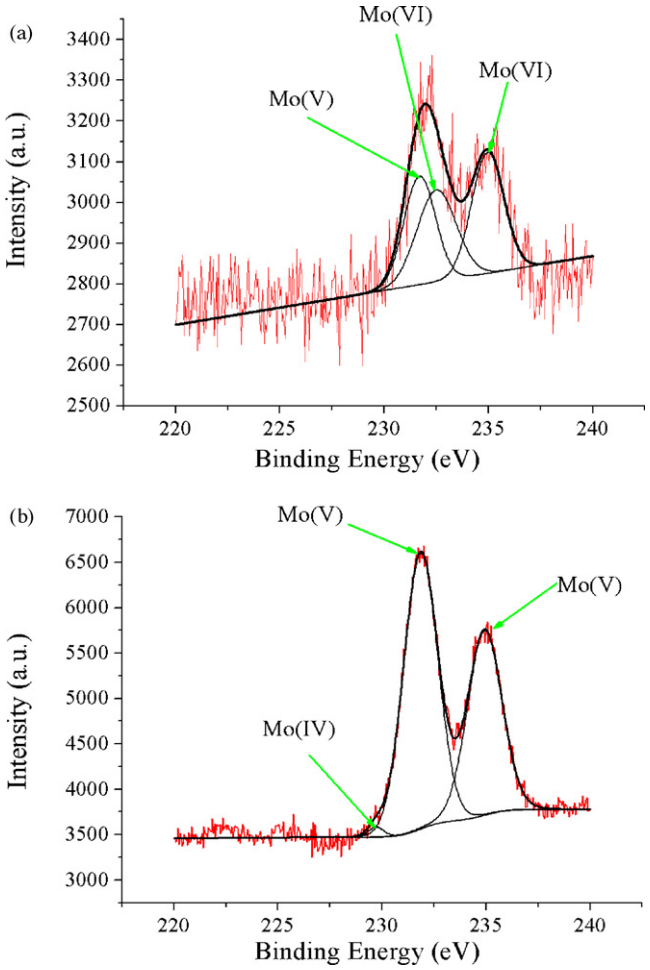

Fig. 6. XPS of Mo3d peaks for as-sintered and H_2-reduced samples.

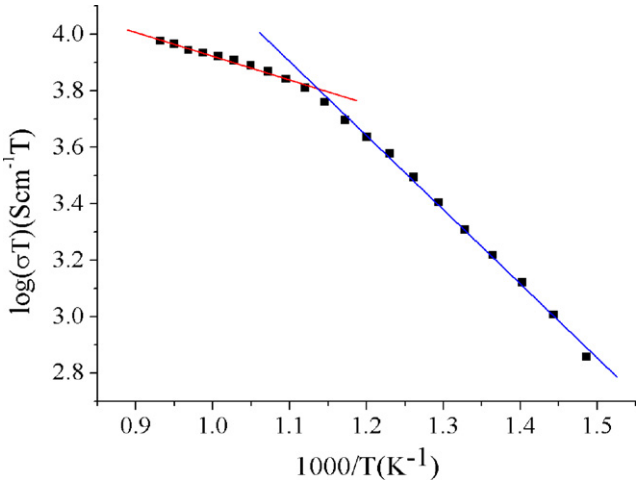

Fig. 7. The Arrhenius plot of SMMO rectangular bar in 5% H_2/Ar.

3.3. XPS analysis of as-sintered and H_2-reduced samples

XPS analysis of as-sintered and H_2-reduced samples for Mo3d are shown in Fig. 6. High-resolution Mo3d spectra show a doublet ($Mo3d_{5/2}$ and $Mo3d_{3/2}$) with asymmetrical peaks. The peaks at 232.7 and 235.8 eV correspond to Mo (VI), whereas Mo (V) lies between 231.7 and 234.9 eV, Mo (IV) is around 229.1 and 232.3 eV, depending on the literatures [11,12]. Hence, the spectral lines at 232.5 and 235.5 eV of Fig. 6(a) are assigned to Mo^{6+}, the spectral line at 231.7 eV is classified to Mo^{5+}. The molar percentage of Mo^{5+} and Mo^{6+} are estimated to be 48.8% and 51.2% respectively. After reduced in 5% H_2/Ar at 800 °C for 10 h, Mo^{6+} line disappears, while three new spectral lines at 229.3, 231.9 and 234.9 eV show up. The three additional low energy lines denote the presence of Mo in lower valence. The spectral lines at 231.9 and 234.9 eV could be attributed to Mo^{5+} and 229.3 eV is Mo^{4+}, as shown in Fig. 6(b). The molar ratio of Mo^{4+} and Mo^{5+} is about 1.7:98.3. Those demonstrate that Mo in the as-sintered SMMO has been reduced after exposure to H_2.

3.4. Electrical properties

The Arrhenius plot of the SMMO rectangular bar in the temperature range of 400–800 °C in 5% H_2/Ar is shown in Fig. 7. It can be seen that the conductivity of SMMO enhances with temperature increasing and reaches the maximum value at 800 °C due to the activation of lattice oxygen. The maximum conductivity value in this work is 8.64 S cm^{-1} at 800 °C, which is slightly higher than 8.60 S cm^{-1} of reported by Huang [7].

It is well established that temperature dependence of conductivity can be described by a small-polaron hopping mechanism:

$$\sigma = \left(\frac{A}{T}\right) \exp\left(\frac{-E_a}{kT}\right)$$

where $E_a = \Delta H_m + \Delta H_t/2$ is the sum of the motional enthalpy ΔH_m of the polarons and the enthalpy ΔH_t to free a Mo (V) from the oxygen vacancy that creates [7]. The activation energy (E_a) can be calculated from the slope of Fig. 7, which shows almost a straight line and there is a turning point at 640 °C. This means that the activation energy has changed at 640 °C. The calculated activation energies at lower temperatures (400–640 °C) and higher temperatures (640–800 °C) are about 21.43 and 6.59 kJ mol^{-1}, respectively. At lower temperatures, the average valences of Mo are high, there exists only a small amount of small-polarons. So the activation energy is larger. With increasing temperatures, the amount of small-polaron increases and the activation energy becomes small.

It is well documented that SMMO possesses high redox, chemical stability and electrocatalytic activity in reducing atmosphere in literatures [7,8]. The above results show that the synthesized double-perovskite SMMO material could be used as a good anode material for SOFC.

4. Conclusions

Nano-crystalline $Sr_2MgMoO_{6-\delta}$ (SMMO) powders have been synthesized by a novel sol–gel thermolysis method. Well-crystallized double-perovskite SMMO can be obtained by calcination at 1450 °C for 12 h. TEM image of SMMO powders demonstrates that the particle size ranges from 50 to 100 nm. SAED pattern shows that SMMO powders are well-developed polycrystalline. Raman spectroscopy is in good agreement with $A(B'_{0.5}B''_{0.5})O_3$ type complex perovskite structure. XPS results show that Mo ions in SMMO have been reduced after exposure to H_2. The conductivity of 8.64 S cm^{-1} is obtained in 5% H_2/Ar at 800 °C, and the activation energies calculated at lower temperatures (400–640 °C) and higher temperatures (640–800 °C) are about 21.43 and 6.59 kJ mol^{-1}, respectively. These results indicate that sol–gel thermolysis method is a promising method to synthesize SMMO anode material.

Acknowledgements

This work was supported by National Basic Research Program of China (No. 2007CB936201), the National High Technology Research and Development Program of China (No. 2006AA03Z351), and the Major Project of International Cooperation and Exchanges (Nos. 50620120439, and 2006DFB51000).

References

[1] S.P. Simner, J.P. Shelton, M.D. Anderson, J.W. Stevenson, Solid State Ionics 161 (2003) 11.
[2] B.C.H. Steele, A. Heinzel, Materials for fuel-cell technologies, Nature 414 (2001) 345–352.
[3] N.P. Brandon, S. Skinner, B.C.H. Steele, Recent advances in materials for fuel cells, Annu. Rev. Mater. Res. 33 (2003) 183–213.
[4] B.C.H. Steele, I. Kelly, H. Middleton, R. Rudkin, Solid State Ionics 547 (1988) 28–30.
[5] S.Q. Hui, A.J. Petric, Eur. Ceram. Soc. 22 (2002) 673.
[6] S.W. Tao, J.T.S. Irvine, Nat. Mater. 2 (2003) 320.
[7] Y.H. Huang, R.I. Dass, Z.L. Xing, J.B. Goodenough, Science 312 (2006) 254.
[8] Y.H. Huang, R.I. Dass, J.C. Denyszyn, J.B. Goodenough, Electrochem. Soc. 153 (2006) A1266.
[9] C.B. Lopez, M. Allix, C.A. Bridges, J.B. Claridge, M.J. Rosseinsky, Chem. Mater. 19 (2007) 1035.
[10] R. Ratheesh, M. Wohlecke, B. Berge, T. Wahlbrink, J. Appl. Phys. 88 (2000) 2813.
[11] J.F. Moulder, W.F. Stickle, P.E. Sobol, K.D. Bomben, Handbook of X-ray Photoelectron Spectroscopy, Physical Electronics Inc., Minnesota, 1995, pp. 113.
[12] H. Belatel, H. Al-Kandari, F. Al-Khorafi, A. Katrib, F. Garin, Appl. Catal. A 275 (2004) 141.